LONGITUDINAL MAGNETORESISTANCE OF Ta/FeMn/Ta, Ta/Dy/Ta AND Ta/CoFe/Ta NANOSTRUCTURES CAUSED BY THE SPIN HALL EFFECT

© 2025 R. S. Zavornitsyn[a,b,] *, L. I. Naumova[a,b], M. A. Milyaev[a,b], I. K. Maksimova[a], V. V. Proglyado[a], V. V. Ustinov[a]

[a]*M.N. Mikheev Institute of Metal Physics of the Ural Branch of the Russian Academy of Sciences, Ekaterinburg, Russia*

[b]*Ural Federal University, The Institute of Natural Sciences and Mathematics, Ekaterinburg, Russia*

**e-mail: zavornitsyn@imp.uran.ru*

Received November 15, 2024

Revised December 14, 2024

Accepted December 30, 2024

Abstract. For Ta/$Fe_{50}Mn_{50}$/Ta, Ta/Dy/Ta, and Ta/$Co_{90}Fe_{10}$/Ta nanostructures prepared by magnetron sputtering, a positive longitudinal magnetoresistance due to the spin Hall effect was found. The difference in the magnitude of magnetoresistance and the shape of magnetoresistive curves obtained for nanostructures with layers of metals with different types of magnetic ordering is interpreted under the assumption of different magnitude of purely spin current injected into the magnetics layer.

Keywords: *magnetoresistance, spin Hall effect, spin current, spin accumulation, β-tantalum*

DOI: 10.31857/S03676765250402e6

INTRODUCTION

The use of spin accumulation and spin currents to control the magnetic state of nanostructures by transferring spin momentum to the subsystem of the magnetically ordered layer (SOT - Spin-Orbit Torque) opens up the prospect of creating low-power consumption microelectronics devices [1-4]. One of the mechanisms of non-

equilibrium spin density and spin current generation is the spin Hall effect (SHE - spin Hall effect) [5], which is most prominently manifested in non-magnetic metals (NM) with strong spin-orbit interaction (Pt, Ta, W). An electric current flowing in such a metal leads to the appearance of a transverse pure spin current. With the inverse spin Hall effect (ISHE - inverse spin Hall effect) the spin current causes the appearance of transverse charge current [6-8]. The study of phenomena of purely spin, quantum nature: the spin Hall effect, as well as the SOT effect, is a difficult experimental task due to the weakness of the registered magnetic and electric signals.

In [9], M.I. Dyakonov theoretically showed that in metal films with strong spin-orbit interaction, the existence of nonequilibrium spin density can be detected by galvanomagnetic experiments. The electric current leads to the accumulation of spin density near the film boundaries and, consequently, spin diffusion from the boundaries into the film depth. This spin current, due to ISHE causes the appearance of a charge current, directed in the same way as the original electric current. When an external magnetic field is applied, the spin accumulation at the film boundaries is suppressed and the resistivity of the sample increases. This type of longitudinal positive magnetoresistance was named Hanle magnetoresistance (HMR - Hanle magnetoresistance), by analogy with the magneto-optics effect, and was detected experimentally [10-12].

Another type of magnetoresistance (SMR - spin Hall magnetoresistance) due to the spin Hall effect is observed in nanostructures that contain neighboring layers of ferromagnetic metal (FM) and nonmagnetic metal with strong spin-orbit interaction. SMR manifests itself as an abrupt change in electrical resistivity in the low-field region

upon remagnetization of the ferromagnetic layer and is associated with spin current absorption/reflection processes at the FM/NM interface [13, 14]. The magnitude of the spin current absorbed or reflected by the ferromagnetic layer depends on the mutual orientation of the magnetic moment ($\vec{M}$) of the ferromagnet and the polarization vector ($\vec{S}$) of the spin current generated in the nonmagnetic layer. When the configuration is orthogonal ($\vec{M} \perp \vec{S}$), the spin current is absorbed and the electrical resistance of the nanostructure $R_{\perp}$ corresponds to the high-resistance state. In the collinear configuration ($\vec{M} \parallel \vec{S}$), spin current reflection occurs at the FM/NM interface. In this case, the reflected spin current due to ISHE leads to a decrease in the electrical resistance of the nanostructure ($R_{\parallel}$). Thus, $R_{\perp} > R_{\parallel}$ [15].

The main characteristics of materials in which SHE is observed are the spin Hall angle ($_{\Theta(SH)}$), which describes the magnitude of the conversion between the charge and spin currents, and the spin diffusion length, which characterizes the distance at which the spin current decays. Ta thin films typically have two structural allotropic modifications: α-Ta, with a volume-centered cubic structure, and β-Ta, which has a tetragonal crystal lattice and a large resistivity. Due to the relatively large value of $_{\Theta(SH),}$ β-Ta is of interest for the synthesis of nanostructures whose magnetic state can be changed by electric current.

In the present work, an experimental study of the galvanomagnetic properties of β-tantalum thin films and nanostructures containing β-tantalum layers and materials with different types of magnetic ordering has been carried out. The difference in the magnetoresistance and the shape of the magnetoresistive curves obtained for different

samples are interpreted under the assumption of different magnitudes of the pure spin current injected into the magnetics layer.

EXPERIMENT

β-Ta films with thicknesses t_{Ta}= 4 - 570 nm, Ta(4nm)/ $Fe_{50}Mn_{(50)}$(2nm)/Ta(4nm) nanostructures, Ta(4nm)/Dy($t_{(Dy)}$)/Ta(4nm), where t_{Dy}= 2, 10, 30 nm, and Ta(4nm)/$Co_{90}Fe_{(10)}$(2nm)/Ta(4nm), were fabricated by magnetron sputtering on glass substrates. The sputtering was carried out at room temperature and 100 W power. The pressure of the working gas (argon) was 0.1 Pa with a base pressure of residual gases in the sputtering chamber of ~ $5\cdot 10^{-7}$Pa. The above sputtering conditions promote the formation of high resistivity allotropic modification of β-tantalum in tantalum films [16-18].

The micro-objects in the form of Hall bridges were fabricated by photolithography (Fig. 1). The microstrip width d ~ 200 μm, the distance between current contacts (1 and 2) ~ 2700 μm, the distance between potential contacts (3 and 4) ~ 2200 μm. The light magnetization axis (LMA) is perpendicular to the microstrip (co-directional to the y-axis). The field dependences of electrical resistivity for the investigated nanostructures were measured at collinear configuration of the applied magnetic field($\vec{H}$) and electric current direction ($\vec{j}$) in the field range ±20 kE in the temperature range 80-293 K.

Magnetoresistance (MR) was defined as $[(R(H) - R(0))/R(0)]\cdot 100\%$

where $R(H)$ and $R(0)$ are the resistivity of the samples in the H field and in the H = 0 field, respectively. The microstructure was investigated by X-ray diffraction.

RESULTS AND DISCUSSION

Microstructure study

No structural peaks are observed in the diffractograms obtained from tantalum films with thicknesses t_{Ta}< 14 nm. At t_{Ta}= 14 nm, a very weak reflex appears, the intensity of which increases with increasing film thickness up to 30 nm (Fig. 2). This peak corresponds to the (002) plane family of the tetragonal crystal structure of β-tantalum. At t_{Ta}= 57 nm, the reflexes (002) and (004) of the tetragonal structure and a weak peak close in location to the reflexes (202) of β-Ta or (110) of α-Ta are present in the diffractogram. Previously [19, 20], we investigated the microstructure and electrical conductivity of tantalum films sputtered under our process conditions and found tetragonal crystal structure, high resistivity and negative temperature coefficient of resistance inherent to β-tantalum. For the present studies, it is important to note that for Ta/FeMn/Ta, Ta/Dy/Ta, and Ta/CoFe/Ta nanostructures, the electrical resistivity increases with decreasing temperature, i.e., the average temperature coefficient of electrical resistivity for the nanostructure is negative.

To investigate the microstructure of the dysprosium layers, diffractograms (Fig. 3) were obtained from Ta(4nm)/Dy($t_{(Dy)}$)/Ta(4nm) nanostructures in which tantalum layers are required to protect the chemically active dysprosium.

As shown above, at a layer thickness of 4 nm the reflections from tantalum are not visible in the diffractograms. In the diffractogram obtained from a sample with a dysprosium layer with a thickness of t_{Dy}=30 nm, there are reflections (10-10) and (0002) of the hexagonal densely packed (HPU) structure of dysprosium. At t_{Dy}=10 nm,

two weak peaks are present in the diffractogram. One of them belongs to the planes (0002) of the GPU, and the second one corresponds to the reflection from the family of planes (111) of the face-centered cubic (HCC) structure. In dysprosium films obtained by magnetron sputtering on a buffer layer of tantalum at room temperature, the formation of a metastable HCC phase near the buffer layer has been observed previously [21, 22]. In these works, it is shown that the magnetic properties of the HCC phase differ significantly from those of bulk dysprosium and films having a conventional GPU structure. In particular, the transition to the ferromagnetic state in the HCC phase of dysprosium occurs at a higher temperature, and the formation of antiferromagnetic ordering is suppressed due to microstresses caused by the proximity of the tantalum buffer layer.

Thus, in tantalum films with a thickness of 4 nm, according to the microstructure studies and earlier estimates of electrical conductivity, a high-resistance β-Ta modification is formed. For dysprosium layers in the Ta(4nm)/Dy(2nm)/Ta(4nm) nanostructure, based on diffractometric studies and data [21, 22] on the magnetic properties of the HCC phase, we can conclude that there is a HCC phase in dysprosium. In this case, the transition from the paramagnetic to the ferromagnetic state is possible at a temperature much higher than the Curie point of bulk dysprosium and without the formation of antiferromagnetic ordering.

Longitudinal magnetoresistance of Ta/FeMn/Ta and Ta/Dy/Ta nanostructures

In the temperature range under study, the antiferromagnetic FeMn layer in the Ta(4nm)/FeMn(2nm)/Ta(4nm) nanostructure may contain uncompensated magnetic

moments that are affected by the external magnetic field due to its small thickness [23]. According to [24], in the Ta(4nm)/Dy(2nm)/Ta(4nm) nanostructure, the dysprosium layer is in a paramagnetic state. Nevertheless, in the case of the transition of the cubic phase of dysprosium into the ferromagnetic state [21, 22], it is possible that a non-zero magnetic moment appears and, accordingly, the magnetic state of the Ta/Dy/Ta nanostructure changes under the field action.

The field dependences of magnetoresistance were obtained at different fixed temperatures for Ta(4nm)/FeMn(2nm)/Ta(4nm) and Ta(4nm)/Dy(2nm)/Ta(4nm) structures, as well as for individual 4nm thick tantalum films. The field was applied in the plane of the film, parallel to the current and perpendicular to the vector of antiferromagnetism in the FeMn layer. Figure 4 shows the field dependences of magnetoresistance at $T = 90$ K.

The magnetoresistance of the β-Ta(4nm) thin film increases with increasing external magnetic field. This is due to the suppression of spin accumulation at the β-Ta boundaries (Hanle magnetoresistance). Experimental and theoretical studies of Hanle magnetoresistance in free β-Ta films of different thicknesses were carried out in [20]. It was shown that the magnitude of longitudinal magnetoresistance depends significantly on the conditions of spin accumulation at the film boundaries.

In Ta/FeMn/Ta, and Ta/Dy/Ta structures, one of the boundaries of each β-Ta(4nm) layer neighbors FeMn(2nm) or Dy(2nm) magnetics having different magnetic ordering. Accordingly, the conditions for spin diffusion across the interface between tantalum and the neighboring layer and for the accumulation of spin density at the boundaries of Ta layers are different for Ta/FeMn/Ta, and Ta/Dy/Ta.

The magnetoresistive curves of the Ta/FeMn/Ta structure and the β-Ta film differ in shape, but the magnitudes of the maximum magnetoresistance in a field of 20 kE practically coincide (Fig. 4). If we consider the β-Ta(4nm) layers in the above nanostructure as two parallel conductors, without taking into account the effects at the boundary with another magnet, then the magnitude of their total relative magnetoresistance is equal to the relative magnetoresistance of one free β-Ta(4nm) film. Hall bridges were lithographically fabricated so that, when the current flows, the spin polarization vector at the boundary of the tantalum layer is collinear to the antiferromagnetism vector in the FeMn layer. In such a case, the spin current originated in β-Ta due to SHE is preferentially reflected at the Ta/FeMn interfaces. If this reflection occurs without spin flipping, the spin density at the β-Ta interfaces increases. These considerations are consistent with the fact that in fields less than 20 kE the magnetoresistance of the Ta/FeMn/Ta structure is larger than for an isolated Ta film.

Due to the small thickness of the layer, the magnetic sublattices in antiferromagnetics are not fully formed, and the increasing magnetic field deforms them. In this case, the conditions of reflection/passage of the spin current through the Ta/FeMn interface and spin flip at reflection change, and the steepness of the $MR(H)$ dependence decreases. In [25], magnetoresistive curves close in shape were obtained for FeMn/Pt bilayer nanostructures, in which the antiferromagnetic and metal layers with strong spin-orbit interaction are also neighboring.

In the Ta(4nm)/Dy(2nm)/Ta(4nm) nanostructure, the angle of deviation of the spin polarization vector of conduction electrons from the local magnetic moments in

paramagnetic Dy varies in a wide range. Accordingly, most of the spin current passes through the Ta/Dy interfaces, which reduces the spin accumulation at the β-Ta interfaces and, consequently, the Hanle magnetoresistance. These considerations are in agreement with the experimental results: for Ta(4nm)/Dy(2nm)/Ta(4nm), the obtained magnetoresistance values are much smaller than for the β-Ta film and the Ta/FeMn/Ta structure (Fig. 4).

Temperature dependences of Hanle magnetoresistance for Ta/FeMn/Ta and Ta/Dy/Ta nanostructures

The field dependences of the longitudinal magnetoresistance were measured at various fixed temperatures in the temperature range 80 - 293 K. In the investigated field range from -20 to 20 kE, none of the $MR(H)$ dependences reached saturation, so the value of the maximum magnetoresistance was estimated as the magnetoresistance in field H = 20 kE. The obtained temperature dependences of the maximum magnetoresistance MR(20KE) are shown in Figure 5. The maximum magnetoresistance of β-Ta(4nm) film monotonically decreases with increasing temperature. Similar dependences were also observed for platinum thin films [10, 11]. A probable explanation for the decrease in magnetoresistance with increasing temperature is the decrease in the spin relaxation time and, consequently, the spin diffusion length.

For the Ta/FeMn/Ta structure, a monotonic decrease of the maximum Hanle magnetoresistance with increasing temperature is also observed; however, in this case, the slope of the dependence is smaller than for the free β-Ta film.

For the Ta/Dy/Ta structure, the character of the dependence of the maximum magnetoresistance on temperature qualitatively differs from the dependences obtained for β-Ta and the Ta/FeMn/Ta nanostructure. At $T>$ 90 K, the magnetoresistance increases with decreasing temperature, which is logically explained by the increase in the spin relaxation time and spin diffusion length. However, at $T <$ 90 K, the temperature decrease is accompanied by a decrease in the value of the maximum magnetoresistance rather than an increase. A possible explanation is that near $T \approx$ 90 K the formation of ferromagnetic ordering begins in the HCC phase of the dysprosium layer [21, 22]. Local magnetic moments in dysprosium line up along the applied magnetic field and, accordingly, perpendicular to the spin polarization vector ($\vec{M} \perp \vec{S}$). At , the spin current passes through the Ta/Dy interfaces, and the spin accumulation at the β-Ta layer boundaries and the Hanle magnetoresistance in the Ta/Dy/Ta nanostructure decrease. Note that the spin Hall effect in Ta layers surrounding dysprosium leads to the accumulation of electrons with opposite spins near the opposite boundaries of the Dy layer. The combination of this character of spin density nonequilibrium and high permeability of Ta/Dy interfaces for the spin current is very likely to lead to intensive spin diffusion through the dysprosium layer in the Ta/Dy/Ta nanostructure.

Longitudinal magnetoresistance of Ta/CoFe/Ta nanostructures

Separately, we will focus on experimental studies of galvanomagnetic properties of a nanostructure containing neighboring layers of non-magnetic metal β-Ta and ferromagnetic alloy $Co_{90}Fe_{10}$.

Figure 6 shows the field dependence of longitudinal magnetoresistance and electrical resistivity for the Ta(4nm)/CoFe(2nm)/Ta(4nm) nanostructure at T = 83 K.

The curve shows a weak increase in the electrical resistance of the sample ($MR \sim 10^{-3}$%) with increasing the field from 0 to 20 kE. This phenomenon is related to the suppression of electron spin accumulation in the external magnetic field and can be interpreted as Hanle magnetoresistance. The sharp decrease in electrical resistance ($MR \sim 10^{-2}$%) of the Ta/CoFe/Ta structure in the region of small fields also attracts attention, which is associated with a change in conditions for spin accumulation in the β-Ta layers due to their neighborhood with the ferromagnetic CoFe layer. Such character of the electrical resistivity change is due to the process of remagnetization of the magnetic moment $\vec{M}$ of the CoFe ferromagnetic layer and can be interpreted as SMR (Fig. 7).

The charge current flowing in the sample plane (collinear to the x-axis) due to SHE induces a purely spin current collinear to the z-axis. This leads to spin accumulation of electrons with spin polarization $\vec{S}$ (collinear to the y-axis) at the interfaces of Ta nanolayers. In this case, interfacial spin mixing occurs at the interfaces Ta/CoFe and part of the spin current is absorbed by the layer of ferromagnetic CoFe. The magnitude of the absorbed spin current is maximum in the case of orthogonal orientation of magnetization $\vec{M}$ and spin polarization of accumulated electrons $\vec{S}$ ($\vec{M} \perp \vec{S}$). This configuration is realized in fields $|\vec{H}| > 50$ Å. As $|\vec{H}|$ decreases to $H \approx 0$, the configuration of $\vec{M}$ and $\vec{S}$ changes from orthogonal to collinear ($\vec{M} \parallel \vec{S}$). In this case, the magnitude of the absorbed spin current is minimal, which due to ISHE contributes to the reduction of the electrical resistance of Ta layers.

It is worth noting that in the case of measuring the longitudinal magnetoresistance of the Ta(4nm)/CoFe(2nm)/Ta(4nm) structure, one can expect to observe not only HMR and SMR, but also anisotropic magnetoresistance (AMR - anisotropic magnetoresistance). The maximum value of AMR is observed at collinearity of magnetization vectors $\vec{M}$ and electric current density $\vec{j}$, and the minimum value is observed at orthogonality $\vec{M}$ and $\vec{j}$.

In order to exclude the contribution of anisotropic magnetoresistance to the total magnetoresistance of the Ta/CoFe/Ta structure, the field dependence of the electrical resistivity was measured at T = 83 K when the external magnetic field is oriented orthogonally to the film plane ($\overrightarrow{H_z}$). It is expected that in this experimental setup, as in the case of longitudinal magnetoresistance measurement ($\overrightarrow{H_x}$), we will observe HMR and SMR as the configurations $\vec{H} \perp \vec{S}$ and $\vec{M} \perp \vec{S}$, respectively, are realized. In this case, the contribution of AMR to the total magnetoresistance of the sample will be minimal ($\vec{M} \perp \vec{j}$).

Figure 8 shows the field dependences of electrical resistivity and magnetoresistance for the Ta(4nm)/CoFe(2nm)/Ta(4nm) nanostructure measured at the orientations of the external magnetic field along the coordinate axes x and z. When increasing $|\vec{H}|$ from 0 to 20 kE, two regions can be distinguished on the field dependence of the longitudinal magnetoresistance - a sharp growth of magnetoresistance due to the remagnetization of ferromagnetic CoFe(2nm) in the plane, and a subsequent weak growth of magnetoresistance with increasing magnetic field, associated with the suppression of spin accumulation in Ta layers.

For the orientation of the magnetic field orthogonal to the film plane, a monotonic increase in the electrical resistivity with increasing external magnetic field is observed. Probably, the shape of the magnetoresistive curve is caused by the escape from the film plane of the magnetic moment of the ferromagnetic layer CoFe(2nm) and the action of demagnetizing fields, and the configuration$\vec{M} \perp \vec{S}$, necessary for the observation of the maximum SMR value, is realized in the fields$|\vec{H}|$ > 15 kE. In this situation, it is more difficult to separate the HMR and SMR contributions due to the remagnetization features of CoFe(2nm). However, it is important to note, at $H \approx 0$, the electrical resistivity of the sample at$\overrightarrow{H_x}$ and$\overrightarrow{H_z}$ was the same, and the maximum magnetoresistance measured at magnetic field orientation along the z axis ($\overrightarrow{H_z}$) increased compared to the maximum longitudinal magnetoresistance ($\overrightarrow{H_x}$). In case of a significant contribution of AMR to the total magnetoresistance of the structure, the opposite situation would be observed. In this case, the large magnetoresistance value obtained for$\overrightarrow{H_z}$, is related to the action of the Lorentz force, which deflects conduction electrons from the electric field direction, increasing the conductor resistivity with increasing magnetic field [26].

Thus, we can conclude that the longitudinal magnetoresistance of the Ta(4nm)/CoFe(2nm)/Ta(4nm) nanostructure is due to two mechanisms - suppression of spin accumulation in β-Ta(4nm) nanolayers (HMR) and absorption/reflection of spin current at the Ta/CoFe interfaces during remagnetization of the magnetic moment of the CoFe(2nm) layer (SMR).

CONCLUSION

In Ta/CoFe/Ta, Ta/FeMn/Ta, and Ta/Dy/Ta nanostructures containing materials with different types of magnetic ordering, positive longitudinal magnetoresistance has been found. It is shown that the character of the observed field and temperature dependences of magnetoresistance is due to changes in the magnetic state of magnetics and, accordingly, in the conditions of reflection/absorption of spin current and accumulation of spin density at the boundary of tantalum layers.

In Ta/FeMn/Ta and Ta/Dy/Ta nanostructures, the longitudinal magnetoresistance arises due to the suppression by the magnetic field of the nonequilibrium spin density at the boundaries of tantalum films and is inherently Hanle magnetoresistance.

For the Ta/FeMn/Ta nanostructure at temperatures above 120 K, the Hanle magnetoresistance is larger for the free β-Ta film. This is explained by the fact that the spin polarization vector of conduction electrons accumulated at the interface of the Ta layer is collinear to the antiferromagnetism vector in the FeMn layer, and in the Ta/FeMn interfaces the reflection of spin current into the β-Ta layer prevails over its passage into the FeMn layer.

For the Ta/Dy/Ta nanostructure, the Hanle magnetoresistance is much lower than that for the β-Ta film. The passage of spin current from the Ta layer and the Dy layer prevails over the reflection back to tantalum, so the spin accumulation at the β-Ta boundaries and, consequently, the Hanle magnetoresistance decreases. In the Ta/Dy/Ta nanostructure, a transverse pure spin current is likely to arise.

The longitudinal magnetoresistance of the Ta/CoFe/Ta nanostructure is due to two mechanisms - suppression of spin accumulation in β-Ta nanolayers and absorption/reflection of the spin current at the Ta/CoFe interfaces during remagnetization of the magnetic moment of the CoFe layer. The contribution of the anisotropic magnetoresistance to the total magnetoresistance of the structure is insignificant.

FUNDING

This work was supported by the grant of the Russian Science Foundation (RNF № 24-12-20022).

REFERENCES

1. *Ando K.* // Proc. Japan. Acad. Ser. B. 2021. V. 97. P. 499.
2. *Go D., Jo D., Lee H.-W. et al.* // Europhys. Lett. 2021. V. 135. Art. No. 37001.
3. *Trushin A.S., Kichin G.A., Zvezdin K.A.* // Bull. Russ. Acad. Sci. Phys. 2023. V. 87. P. 88.
4. *Morgunov R.B., Bakhmetiev M.V., Chernov A.I. et al.* // JETP Lett. 2024. V. 119. P. 299.
5. *D'yakonov M.I., Perel' V. I. //* JETP Lett. 1971. V. 13. P. 467.
6. *Chazalviel J.-N.* // Phys. Rev. B. 1975. V. 11. P. 3918.
7. *Kato Y.K., Myers R.C., Gossard A.C. et al.* // Science. 2004. V. 306. P. 1910.
8. *Niimi Y., Suzuki H., Kawanishi Y. et al.* // Phys. Rev. B. 2014. V. 89. Art. No. 054401.
9. *Dyakonov M.I.* // Phys. Rev. Lett. 2007. V. 99. Art. No. 126601.
10. *Vélez S., Golovach V.N., Bedoya-Pinto A. et al.* // Phys. Rev. Lett. 2016. V. 116.

Art. No. 016603.

11. *Wu H., Zhang X., Wan C.H. et al.* // Phys. Rev. B. 2016. V. 94. Art. No. 174407.

12. *Li J., Comstock A.H., Sun D. et al.* // Phys. Rev. B. 2022. V. 106. Art. No. 184420.

13. *Meng K., Xiao J., Wu Y. et al.* // Sci. Reports. 2016. V. 6. Art. No. 20522.

14. *Kim J., Sheng P., Takahashi S. et al.* // Phys. Rev. Lett. 2016. V. 116. Art. No. 097201.

15. *Althammer M., Meyer S., Nakayama H. et al.* // Phys. Rev. B. 2013. V. 87. Art. No. 224401.

16. *Abadias G., Colin J.J., Tingaud D. et al.* // Thin Solid Films. 2019. V. 688. Art. No. 137403.

17. *Ellis E.A.I., Chmielus M., Baker S.P. et al.* // Acta Mater. 2018. V. 150. P. 317.

18. *Magnuson M., Greczynski G., Eriksson F. et al.* // Appl. Surf. Sci. 2019. V. 470. P. 607.

19. *Naumova L.I., Zavornitsyn R.S., Milyaev M.A. et al.* // Phys. Metals. Metallorg. 2023. V. 124. P. 763.

20. *Ustinov V.V., Naumova L.I., Zavornitsyn R.S., et al. //* ZHETF. 2024. T. 165. C. 114.

21. *Scheunert G., Hendren W.R., Lapicki A.A. et al.* // J. Physics D. Appl. Phys. 2013. V. 46. Art. No. 152001.

22. *Scheunert G., Ward C., Hendren W.R. et al.* // J. Physics D. Appl. Phys. 2014. V. 47. Art. No. 415005.

23. *Yang Y., Xu Y., Zhang X. et al.* // Phys. Rev. B. 2016. V. 93. Art. No. 094402.

24. *Naumova L.I., Bebenin N.G., Zavornitsyn R.S. et al.* // Phys. Metals. Metall. 2023.

V. 124. P. 1768.

25. *Yang Y., Xu Y., Yao K. et al.* // AIP Advances. 2016. V. 6. Art. No. 065203.

26. *Gorkom R.P., Caro J., Klapwijk T.M. et al.* // Phys. Rev. B. 2001. V. 63. Art. No. 134432.

FIGURE CAPTIONS

Fig. 1. Schematic representation of a micro-object in the form of a Hall bridge.

Fig. 2. Diffractograms obtained for tantalum films with thicknesses of 14, 30 and 57 nm.

Fig. 3. Diffractograms obtained for Ta(4nm)/Dy($t_{(Dy)}$)/ Ta(4nm) nanostructures with dysprosium thickness t_{Dy}= 30 and 10 nm**.**

Fig. 4. Field dependences of longitudinal magnetoresistance for β-Ta(4nm) film as well as Ta(4nm)/FeMn(2nm)/Ta(4nm) and Ta(4nm)/ Dy(2nm)/(4nm) trilayer structures at T = 90 K.

Fig. 5. Temperature dependences of the maximum longitudinal magnetoresistance for the β-Ta(4nm) film, as well as the Ta(4nm)/FeMn(2nm)/Ta(4nm) and Ta(4nm)/Dy(2nm)/(4nm) trilayer structures.

Fig. 6. $R(H)$ and $MR(H)$ dependence for the Ta(4nm)/CoFe(2nm)/Ta(4nm) structure at T = 83 K. The HMR and SMR contributions to the magnetoresistance of the sample are schematically labeled.

Fig. 7. $R(H)$ dependence for the Ta(4nm)/CoFe(2nm)/Ta(4nm) nanostructure in the field range ±100 E at T = 83 K. Inset: schematic representation of Ta/CoFe/Ta

nanostructure, magnetic moment $\vec{M}$ of CoFe ferromagnetic layer and spin polarization $\vec{S}$ of accumulated electrons in Ta.

Fig. 8. Dependences of $R(H)$ and $MR(H)$ for Ta(4nm)/CoFe(2nm)/ Ta(4nm) nanostructure at orientation of external magnetic field along x and z axes.

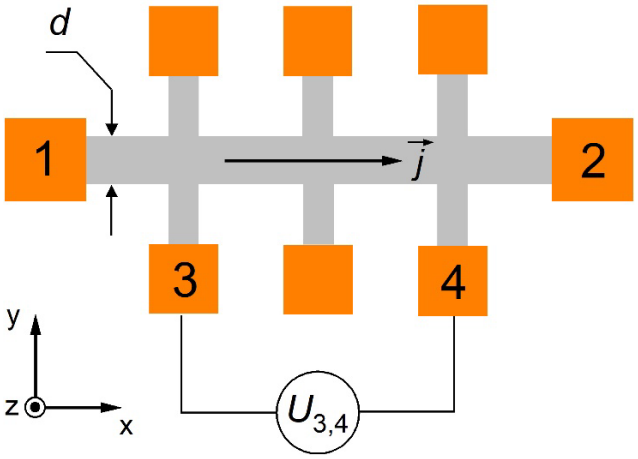

Fig. 1.

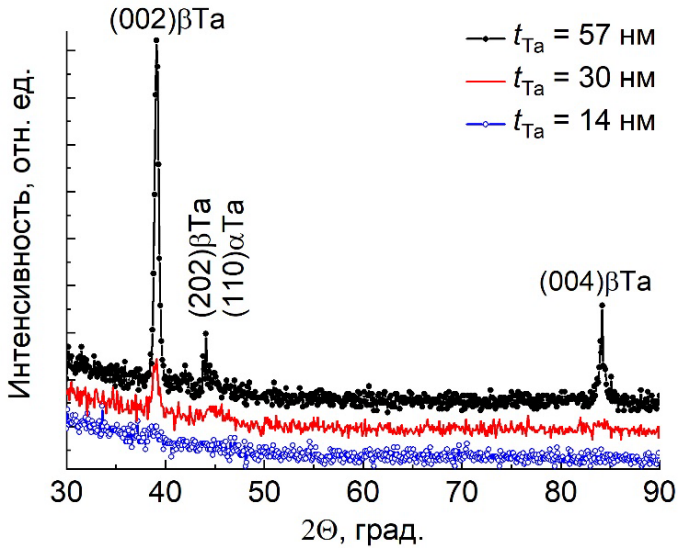

Fig. 2.

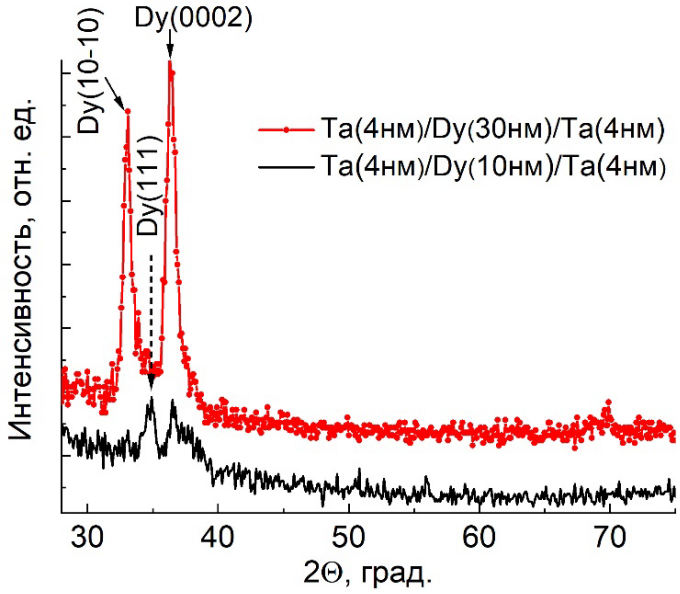

Fig. 3.

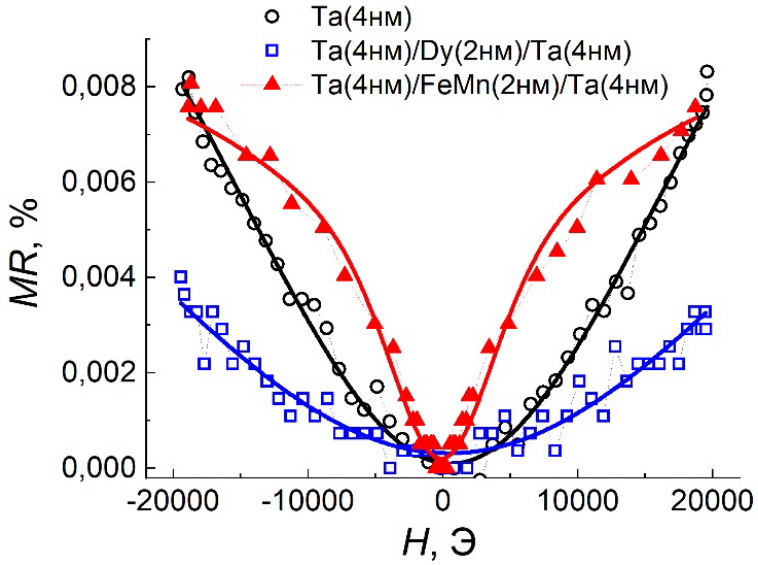

Fig. 4.

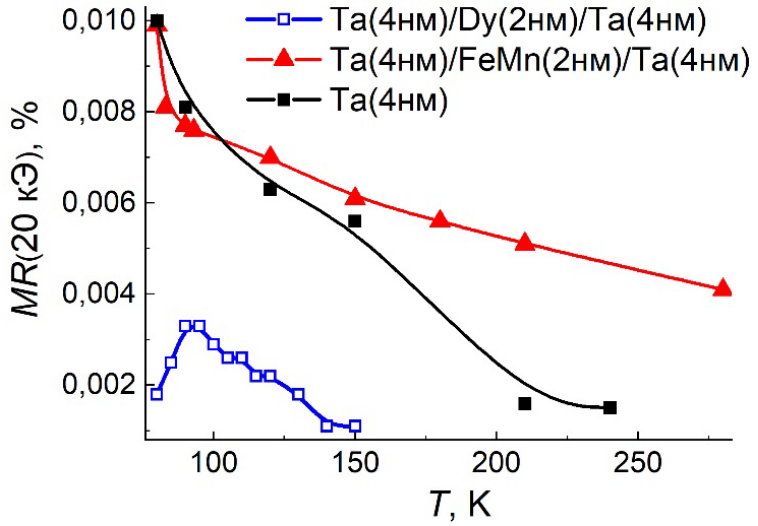

Fig. 5.

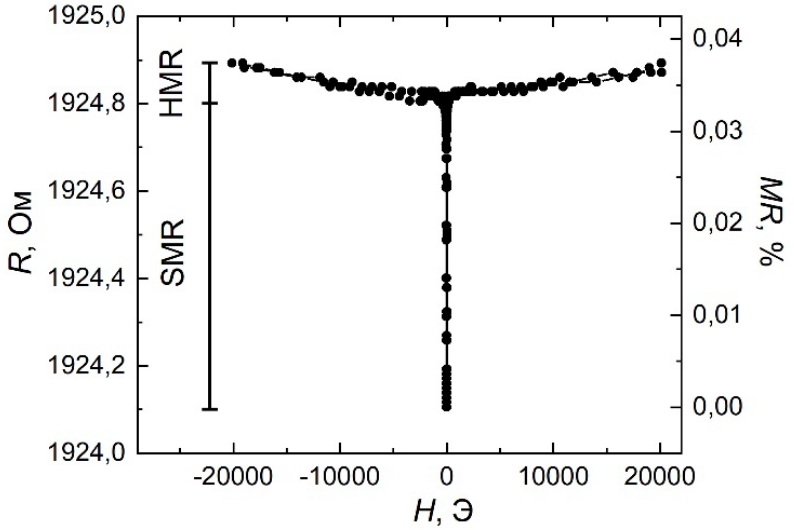

Fig. 6.

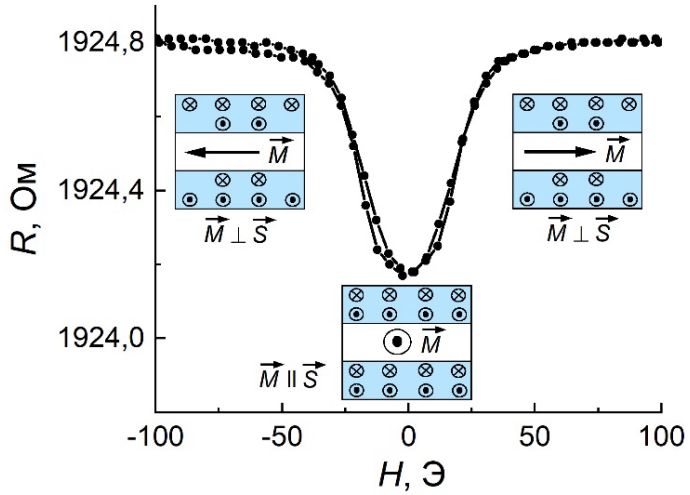

Fig. 7.

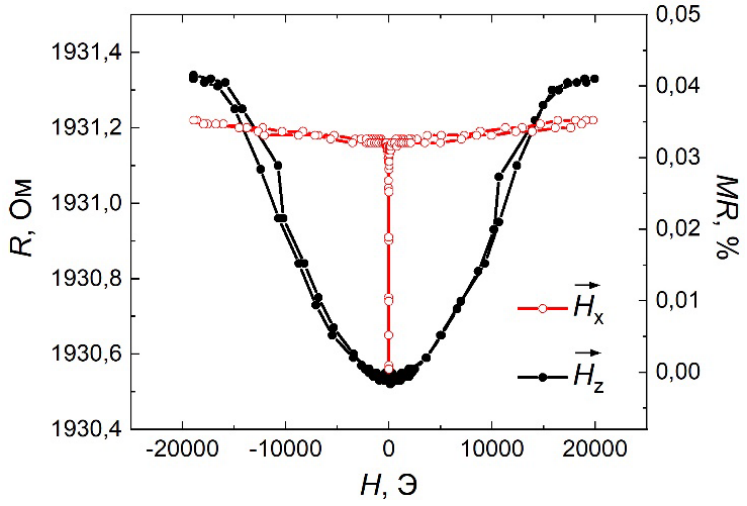

Fig. 8.